

Fast-Poly: A Fast Polyhedral Framework For 3D Multi-Object Tracking

Xiaoyu Li[†], Dedong Liu[†], Yitao Wu[†], Xian Wu[†], Lijun Zhao*, Jinghan Gao

Abstract—3D Multi-Object Tracking (MOT) captures stable and comprehensive motion states of surrounding obstacles, essential for robotic perception. However, current 3D trackers face issues with accuracy and latency consistency. In this paper, we propose Fast-Poly, a fast and effective filter-based method for 3D MOT. Building upon our previous work Poly-MOT, Fast-Poly addresses object rotational anisotropy in 3D space, enhances local computation densification, and leverages parallelization technique, improving inference speed and precision. Fast-Poly is extensively tested on two large-scale tracking benchmarks with Python implementation. On the nuScenes dataset, Fast-Poly achieves new state-of-the-art performance with 75.8% AMOTA among all methods and can run at 34.2 FPS on a personal CPU. On the Waymo dataset, Fast-Poly exhibits competitive accuracy with 63.6% MOTA and impressive inference speed (35.5 FPS). The source code is publicly available at <https://github.com/lixiaoyu2000/FastPoly>.

Index Terms—Multi-Object Tracking, Real-Time Efficiency, 3D Perception

I. INTRODUCTION

3D MULTI-OBJECT TRACKING filters and recalls obstacle observations, being a crucial component in autonomous driving and robot perception systems. Recent advances in 3D MOT can be attributed to the success of the Tracking-By-Detection (TBD) framework¹. Despite the advancements, these filter-based works [1]–[7] currently suffer from the consistency of accuracy and latency on large-scale datasets (nuScenes [8], Waymo [9], etc.), as shown in Fig. 1. Specifically, these datasets mainly bring the proliferation of tracking agents, magnifying four primary shortcomings of filter-based methods:

- **Object is rotated in 3D space.** Geometry-based metrics (IoU [10], [11], GIoU [1], [2], [4]) provide high interpretability and accurately capture inter-object affinity, are widely utilized. However, according to statistics in Table II, 3D object rotation leads to time-consuming polygon intersection and convex hull solution steps in these metrics. Some works [3], [12] employ custom Euclidean distance to reduce overhead, but accuracy is lost due to the lack of spatial relationship considerations.
- **The tracking pipeline is from a global perspective.** Modeling global object similarity for pre-processing and association is a common practice in the field [1]–[4], [10]–[12]. However, inter-observation redundancy and trajectory-observation correlation are only feasible in a

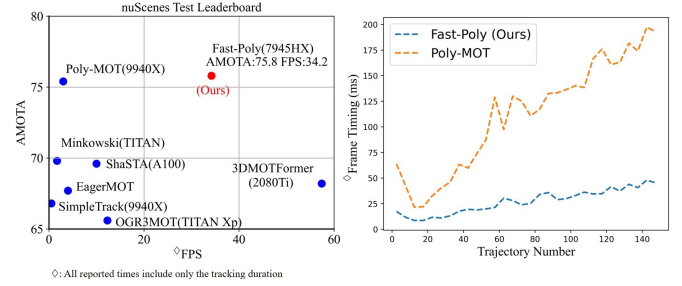


Fig. 1: **Left:** The comparison of the accuracy and latency between our method and advanced trackers on **nuScenes test leaderboard**. The closer to the top right, the better the performance. Fast-Poly also exhibits superior performance on the **Waymo test leaderboard** with 63.6% MOTA and 35.5 FPS. **Right:** The time consumption curve of average frame timing with the objects increasing between our proposed Fast-Poly and baseline method Poly-MOT on nuScenes val set.

limited local space, leading to numerous invalid computations. [1], [2], [4] emphasize restricting false positive (FP) agents from influencing cost computations. [1] also applies multiple criteria to avoid distinct categories matching. Despite these efforts, the fact that *distant objects are unrelated* is widely ignored.

- **Matrix calculations in filters are heavy.** Trajectories typically represented as high-dimensional vectors [1]–[4], [10]–[12]. Nevertheless, integrating time-invariant states in the Kalman Filter (KF) leads to redundant computations involving zeros. [13] accelerates 2D position estimation through a priori split calculation and CUDA operator. However, in 3D MOT, the abundance of states and non-linear motion models [1] make a similar matrix-to-quadratic form transformation challenging. Furthermore, rigid count-based lifecycle management hinders real-time performance due to matrix operations applied to all active tracklets, including the coasted FP tracklets.
- **The TBD framework is serial logic inherently.** Existing methods rely on a module-by-module program execution order due to the extensive fusion calculations between observations and tracklets within the TBD framework. This conventional view overlooks the potential for localized parallel processing, hindering efficiency.

Towards these issues, we propose Fast-Poly, a fast and effective polyhedral framework for 3D MOT. Specifically, to eliminate the object rotation impact, we introduce an elegant solution: Align rotated objects and then employ 2D-like parallel IoU operations for accelerated similarity calculations.

[†]: These authors contributed equally to this work. *: Corresponding author. All authors are with State Key Laboratory of Robotics and System, Harbin Institute of Technology, Harbin 150006, China.

¹Top 5 methods on **nuScenes** are all adhere to the TBD framework.

To avoid invalid global affinity computations, we introduce the voxel mask to calculate valuable costs quickly based on coarse-to-fine criteria. To minimize the KF burden, we first incorporate a lightweight filter to decouple and manage time-invariant states, streamlining the trajectory vectors. Additionally, we propose a confidence-count mixed lifecycle strategy to flexibly terminate the trajectory, mitigating FP tracking agents in the maintenance list. As a practical solution, we parallelize pre-processing and motion prediction based on their independent relationships, alleviating the serial bottleneck.

Fast-Poly is learning-free and can perform fast, accurate tracking with limited resources (only CPU). Fast-Poly builds upon our previous work Poly-MOT [1], an advanced tracker optimized for multi-category scenes. With the Python implementation, Fast-Poly is fully assessed on two autonomous driving datasets (nuScenes [8], Waymo [9]). **On nuScenes, Fast-Poly establishes a new state-of-the-art with 75.8% AMOTA and 34.2 FPS among all methods**, accompanied by a $5\times$ faster inference speed than baseline. On Waymo, Fast-Poly attains competitive performance with 63.6% MOTA and impressive speed (35.5 FPS). Our main contributions include:

- We propose Fast-Poly, a filter-based 3D MOT method that combines high real-time performance with outperform accuracy across two large-scale autonomous driving datasets (nuScenes [8], Waymo [9]).
- We leverage rotated object alignment, local computation densification, and module parallelization techniques to solve the real-time dilemma of filter-based methods while improving accuracy.
- We achieve state-of-the-art tracking performance on the nuScenes test leaderboard among all methods with 75.8% AMOTA and 34.2 FPS.
- Our code is made publicly available, aiming to serve as a strong baseline for the community.

II. RELATED WORK

A. 3D Multi-Object Tracking

Current 3D MOT [1]–[7], [10]–[12], [14]–[19] benefits from advancements in 2D MOT [13], [20]–[22] and 3D detection [19], [23]–[27]. AB3DMOT [10] pioneers the expansion of the TBD framework into 3D space, introducing a simple yet effective baseline. Poly-MOT [1] proposes category-specific ideas to introduce a strong tracker based on multiple non-linear models and similarity metrics, achieving SOTA performance on nuScenes. With Neural Network (NN) and a post-processing manner, some methods [5]–[7], [15] utilize the features output by the pre-trained backbone [19] to regress the affinity or even the tracking confidence [6]. Leveraging the occlusion robustness of LiDAR and the far-sightedness of cameras, EagerMOT [3] performs a detection-level fusion to combine 2D and 3D detectors. CAMO-MOT [2] introduces an occlusion head to classify the visual occlusion status and implements a confidence-involved LiDAR association. Being economical and an end-to-end pipeline, multi-camera trackers [17], [18] receive attention and applications. Following the Tracking-By-Attention (TBA) framework, these trackers

implement spatial-temporal modeling based on self/cross-attention and implicitly learn trajectory motion in a self-refinement paradigm. The trade-off between computational overhead, real-time performance, and tracking accuracy is the primary research direction in the current landscape.

B. Tracking-By-Detection

Core Idea. Taking advanced detection results as input, tracking is handled independently on the tracker-end entirely in a post-processing manner. The TBD framework features a well-established pipeline, dividing 3D MOT into four components: pre-processing, estimation, association, and lifecycle.

Pre-processing. This module recalls high-quality observations from raw detections based on spatial information between detections (Non-Maximum Suppression [1], [2], [4], NMS) or confidence (Score Filter [1], [2], SF). However, the global perspective inherent in the process leads to redundant computations. In contrast, our method employs the voxel mask, effectively bypassing these calculations.

Estimation. This module utilizes filters (Linear Kalman Filter [2]–[4], [10]–[12], Extended Kalman Filter [1], Point Filter [14], [19], etc.), along with motion models, to perform two functions: (1) Predict the alive tracklets to achieve temporal alignment and association with the detection. (2) Update the matched tracklets with the corresponding observations, preparing prior information for downstream. Nevertheless, the real-time challenge emerges when managing numerous tracklets, as the filter involves heavy matrix operations on each tracklet. Therefore, we decouple and filter time-invariant states using a lightweight filter to alleviate the computational burden.

Association. As the core of the system, this module establishes tracklet-observation similarity and resolves matching correspondence. Geometry-based (IoU [10], [11], GIoU [1], [2], [4], Euclidean [3], [12], [14], NN distance [5]–[7], [15], etc.) and appearance-based are the commonly used affinity metrics. The former modeling process, reliant solely on spatial information, is mostly unsupervised and robust to occlusion. The latter, robust to inaccurate depth, can describe distant objects. Under the one-to-one assumption, the optimal assignment [28] algorithm is then used to obtain matching pairs. However, rotation in 3D space impairs the parallelization of IoU-like metrics, introducing severe latency. Fast-Poly proposes to leverage alignment to solve this dilemma.

Lifecycle. This module initializes, terminates, and merges tracklets based on the count-based strategy [1]–[4], [10], [11] or the confidence-based [1], [4], [12], [14] strategy. The former has simple logic and strong robustness. The latter is more flexible in processing based on heuristic functions. In response to the inherent rigidity issue of the former approach, we employ score refinement to flexible terminate trajectories. In addition, we leverage trajectory average scores and a novel prediction to bolster occlusion robustness and enhance the estimation accuracy of the confidence-based strategy.

III. FAST-POLY

A. Overall Architecture

Despite sharing a similar pipeline, Fig. 2 illustrates the distinctions between our proposed method and Poly-MOT [1].

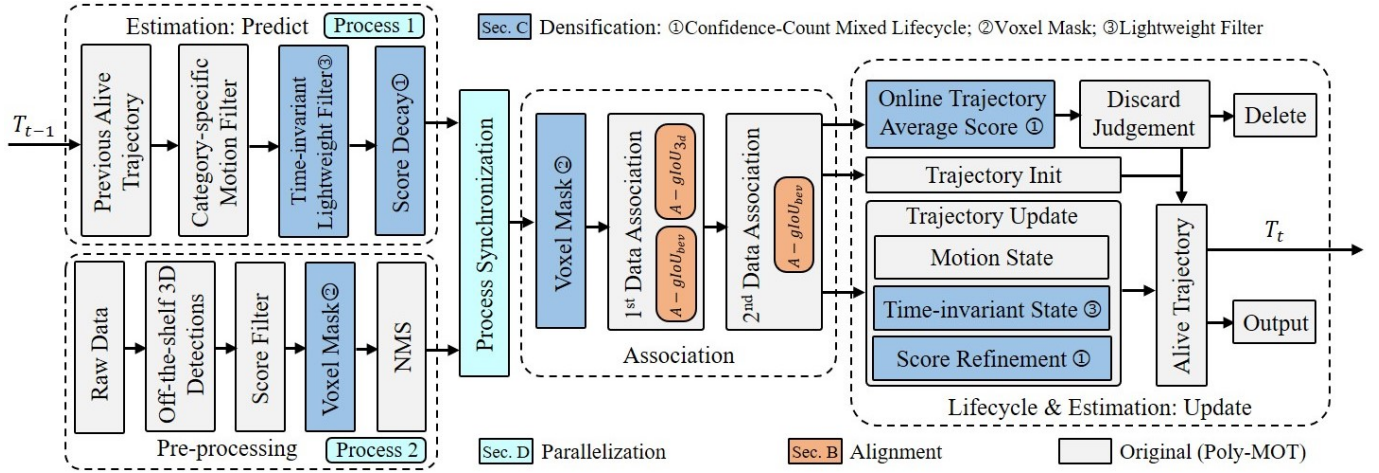


Fig. 2: The pipeline of our proposed method. Our structure design is illustrated in Section III-A. Real-time improvements to the baseline [1] are highlighted in distinct colors. **Orange** denotes the *Alignment* to reduce the computational complexity of affinity calculations for rotated objects. **Blue** denotes the *Densification* to increase computational efficiency. **Cyan** denotes the *Parallelization* to execute pre-processing and motion prediction simultaneously, enhancing computational efficiency.

At each frame t , Fast-Poly employs two independent computing processes (Section III-D) to filter the 3D detections D_t and predict existing trajectories $T_{t,t-1}$. Specifically, SF and NMS filters are leveraged to process the detections. Besides, the motion (time-variable), score (Section III-C1), and time-invariant (Section III-C3) states of trajectories are predicted by corresponding filters. D_t and $T_{t,t-1}$ are then subjected to construct cost matrices for two-stage association. Notably, during NMS and matching, our proposed voxel mask (Section III-C2) and a novel geometry-based metric (Section III-B) accelerate computing. Hungarian algorithm [28] is then employed to obtain matched pairs DT_t , unmatched detections D_t^{um} , unmatched tracklets T_{t-1}^{um} . To relieve the matrix dimension, time-invariant and time-variable states in matched tracklets T_{t-1}^m are updated with corresponding observations D_t^m based on our proposed lightweight filter (Section III-C3) and Extended Kalman Filter (EKF), respectively. T_{t-1}^m scores are also refined leveraging the confidence-count mixed lifecycle (Section III-C1). D_t^{um} are then initialized as newly active tracklets. To flexibly determine FP agents in T_{t-1}^{um} , we soft-terminate the mismatch tracklets by considering their max-age and online average refined scores. The remaining tracklets T_t are sent to downstream tasks and implemented for next frame tracking.

B. Alignment

This section details how Fast-Poly mitigates high latency caused by object rotations through alignment, covering implementation and principles.

GIoU. Without loss of generality, we optimize the widely employed metric in nuScenes SOTA trackers [1], [2] Generalized Intersection over Union $gIoU$, which is formulated as:

$$gIoU(B_i, B_j) = \frac{\Lambda(B_i \cap B_j)}{\Lambda(B_i \cup B_j)} + \frac{\Lambda(B_i \cup B_j)}{\Lambda_{Hull}(B_i, B_j)} - 1, \quad (1)$$

where B is the 3D bounding box representing the detection or tracklet. According to the representation space, $\Lambda(\cdot)$ is the area function in the BEV space and the volume function in

the 3D space. $B_i \cap B_j$, $B_i \cup B_j$ and Λ_{Hull} are the intersection, union and convex hull computed by B_i and B_j , respectively.

A-GIoU. Varied from the pixel plane, the rotation causes overlap and convex hull irregular polygons instead of axis-aligned rectangles. The complexity of the well-known Sutherland-Hodgman [29] and Graham scan [30] algorithm are $\mathcal{O}(n^2)$ and $\mathcal{O}(n \log n)$, where n is the number of input points. In addition, the sum calculation time increases rapidly with the growth of detections and tracklets. On the contrary, the solution complexity of the axis-aligned bounding box is only $\mathcal{O}(n)$. To this end, we proposed the Aligned Generalized Intersection over Union ($A-gIoU$), which is formulated as:

$$A-gIoU(B_i, B_j) = \frac{\Lambda(B_i^A \cap B_j^A)}{\Lambda(B_i^A \cup B_j^A)} + \frac{\Lambda(B_i^A \cup B_j^A)}{\Lambda_{Hull}(B_i^A, B_j^A)} - 1, \quad (2)$$

where B^A represents the axis-aligned B , containing the top-left and bottom-right points $p \in \mathbb{R}^{1 \times 4}$ on the ground plane. Using the Bird's-Eye View (BEV) space as a case study, the alignment procedure is depicted in Fig. 3(d). The overlap and convex hull calculations in Eq. (2) are consistent with $gIoU_{2d}$ [31], with $\mathcal{O}(n)$ computational complexity. For clarity in subsequent discussions, we designate the parts of $gIoU$ and $A-gIoU$ excluding IoU as the *spatial occupancy difference*.

Delving into A-GIoU. As shown in Table II and V, on nuScenes, integrating $A-gIoU$ reduces latency by 73% while enhancing accuracy (+0.5% MOTA). This prompts the question: why does it excel in tracking tasks? A critical insight is that $A-gIoU$ aligns closely with $gIoU$ in describing the similarity between identical object pairs and quantifying the discrepancy between different matching instances.

Take 3D space as an example, firstly, Fig. 3(a) provides intuitive evidence of the similarity consistency between these two metrics for the same bbox pair across various geometric scenarios². Generally, $A-gIoU$ slightly exceeds $gIoU$, with

²Both bboxes use nuScenes *Car* average 3D size, with Z-position fixed at 1m and yaw angle sampled at 1.2° step in $[0^\circ, 180^\circ]$. X-Y positions: Bbox1 at (0m, 0m); Bbox2 is sampled at 1m step in $[-5m, 5m]$.

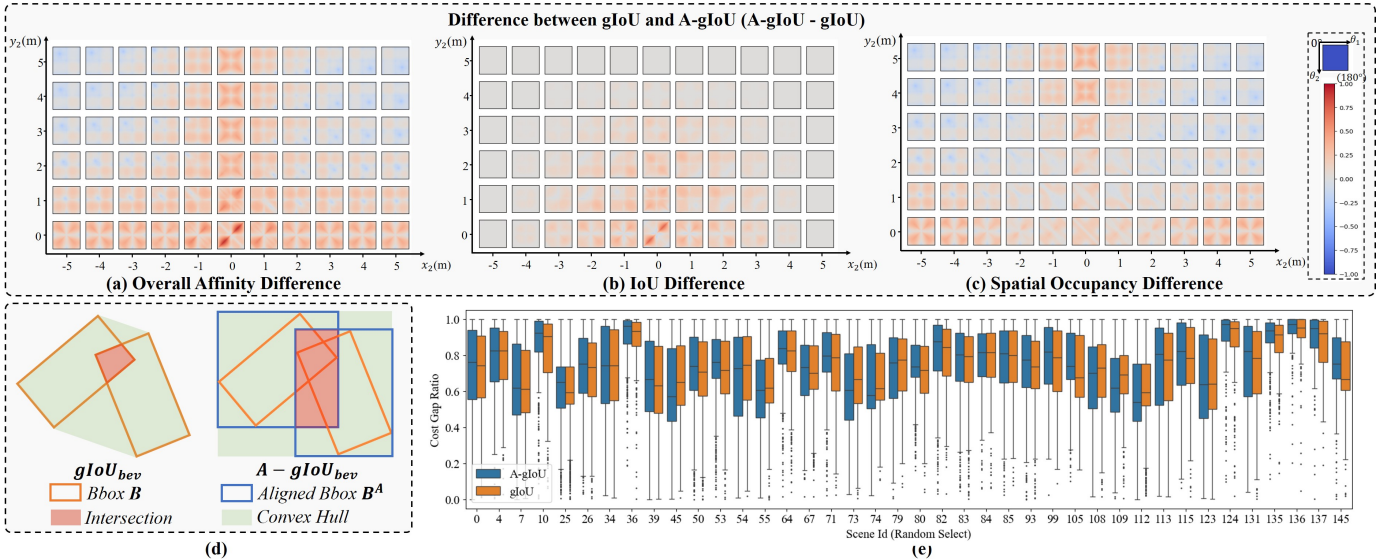


Fig. 3: **Top**: Affinity difference between $A-gIoU$ and $gIoU$ for identical bbox pairs under varying geometric conditions in the 3D space. **(a)**: overall affinity difference. **(b)**: IoU difference. **(c)**: spatial occupancy difference. **Bottom-Left**: The calculation process of distinct metrics in the BEV space. **Bottom-Right**: The contributions of CGR across all trajectories within randomly sampled scenes from nuScenes of $A-gIoU$ and $gIoU$, employing our tracker with CenterPoint [19] detector.

tiny differences in small object overlaps (distant or parallel bbox pairs) cases. To elucidate these phenomena, Fig. 3(b, c) breaks down the distinctions between the two components of both metrics. Fig. 3(c) reveals that *spatial occupancy difference* is the key factor of this consistency. Fig. 3(b) further highlights the source of the minor distinction and the enhancement provided by $A-gIoU$: It increases the IoU for closely positioned bbox pairs, improving the tracker to recall observations with strong positional correlation despite inaccurate heading angles.

Secondly, to validate the consistency between $A-gIoU$ and $gIoU$ in distinguishing true matches from false matches in data association, we introduce the Cost Gap Ratio (CGR) to quantify the performance disparity. CGR is defined as:

$$CGR = (\min(C_{um}) - C_m) / (\max(C_{um}) - C_m), \quad (3)$$

where C_m and C_{um} are the cost of the true match and the false matches for a single tracklet³. A higher CGR indicates a more pronounced difference between C_m and C_{um} , suggesting a higher probability of a true positive match. Fig. 3(e) illustrates CGR values across all trajectories within randomly sampled scenes from nuScenes. The consistency between $A-gIoU$ and $gIoU$ in characterizing distinct matching instances is confirmed by similar Quartile1 (Q1), median, and Quartile3 (Q3) values. In addition, for $A-gIoU$, at least 75% of CGR (Q1) exceeds 0.4 in the sampled scenes, ensuring the matching algorithm constructs accurate and stable bipartite graphs.

C. Densification

In this section, we improve the computational efficiency of the 3D tracking system through three key enhancements: soft tracklet elimination using tracking scores, distant similarity

calculation prevention via the voxel mask, and time-invariant states splitting with a lightweight filter.

Confidence-Count Mixed Lifecycle. Different from the rigid The classic count-based lifecycle seriously raises tracker maintenance costs. In contrast, [14] flexibly terminates tracklets by manipulating scores, significantly reducing FP. However, as evidenced in [14] and Table VI, the deletion based on the latest score and the application of minus prediction detrimentally affect mismatch tracklets due to occlusion or FN detections. Towards this, a power function is first implemented to predict the scores smoothly. The refinement is described in two steps as follows:

$$\begin{cases} \text{Predict: } s_{t,t-1} = \sigma \cdot s_{t-1}, \\ \text{Update: } s_t = 1 - (1 - s_{t,t-1}) \cdot (1 - c_t), \end{cases} \quad (4)$$

where s_{t-1} , $s_{t,t-1}$ and s_t are the $t-1$ frame posterior score, t frame priori score and t frame posterior score of current tracklet, respectively. c_t is the corresponding detection score. σ is the hand-crafted decay rate, empirically ≤ 0.7 . The update function is similar with [14], satisfies that s_t is more confidence than $s_{t,t-1}$ or c_t . After refinement, tracklets are terminated if their online average scores (computed from the initial frame to the current frame) fall below the deletion threshold θ_{dl} or if the number of mismatch frames exceeds the max-age. There are two noteworthy benefits: (1) Tracklets demonstrate increased resilience to temporary occlusions since their average confidence score decays gradually, as depicted in Table VI. (2) The power function swiftly pulls the tracklet predict score to the $[0, \sigma]$ interval, leaving the over-confidence area ($[0.7, 1]$ interval in Fig. 2 of [14]). This reduces the hysteresis in score estimates, improving the tracking performance.

Voxel Mask. In 3D MOT, an overlooked consideration is: *redundancy and matching are improbable between objects separated by significant distances in 3D Euclidean space*. This starkly contrasts inherently no-depth 2D MOT [13], [20]. To

³Outliers ($C_m \geq \min(C_{um})$) are excluded (representing $\leq 3\%$ of data) to constrain CGR within the (0, 1] interval.

address this issue, we propose the voxel mask inspired by the coarse-to-fine idea [32]. Specifically, before computing the global cost during data association and NMS iteration, we employ low-overhead Euclidean distance (2-norm) $\|\cdot\|_2$ and a hand-crafted size parameter θ_{vm} to generate voxel mask. The process can be expressed as:

$$\begin{cases} \text{Coarse: } M_t = (\|\mathcal{B}_1^{xyz} - \mathcal{B}_2^{xyz}\|_2 \leq \theta_{vm}), \\ \text{Fine: } C_t = 1 - \text{Aff}(M_t, \mathcal{B}_1, \mathcal{B}_2), \end{cases} \quad (5)$$

where \mathcal{B} is the 3D bounding boxes representing detections or tracklets based on module representation. \mathcal{B}^{xyz} are the 3D positions. M_t is the voxel mask between \mathcal{B}_1 and \mathcal{B}_2 . $\text{Aff}(\cdot)$ is the affinity function, constructing inter-object similarities between objects in pre-processing and association to detect redundancy and recall observations, respectively. Notably, $\text{Aff}(\cdot)$ directly pads invalid values into false index within M_t to expedite, ultimately yielding C_t .

Lightweight Filter. Current 3D MOT methods embed the time-invariant states (Z-position z , width w , length l , height h) of trajectory into the Kalman Filter. However, the time invariance makes the Jacobian matrices of process and observation identity matrices, resulting in numerous meaningless 0-related calculations. Besides, the computational time escalates swiftly with an expanding number of trajectories. To this end, we decouple these states X^{ti} from the KF and estimate them using a compact filter. The estimate process is expressed as:

$$\begin{cases} \text{Predict: } X_{t,t-1}^{ti} = X_{t-1}^{ti}, \\ \text{Update: } X_t^{ti} = \text{LW-Filter}(X_{t,t-1}^{ti}, D_t^i), \end{cases} \quad (6)$$

where X_{t-1}^{ti} , $X_{t,t-1}^{ti}$ and X_t^{ti} are the $t-1$ frame posterior X^{ti} , t frame priori X^{ti} and t frame posterior X^{ti} of current tracklet, respectively. D_t^i is the corresponding detection. $\text{LW-Filter}(\cdot)$ is the custom lightweight filter, implemented by a median or mean filter with length l_{lw} in Fast-Poly. It stores nearest fixed-size time-invariant trajectory observations for prompt state estimation. There are two key insights: (1) $\text{LW-Filter}(\cdot)$ bypasses invalid computations, enabling fast filtering while preserving temporal data. (2) In contrast to KF, which entails manual process and observation noise, $\text{LW-Filter}(\cdot)$ relies solely on a single hyperparameter l_{lw} , reducing overfitting and ensuring robustness, as proven in Fig. 5.

D. Parallelization

Although the TBD framework is inherently serial, certain modules can be parallelized. Consequently, in Fast-Poly, after tracking in the previous frame, motion estimation prediction and preprocessing are synchronized using multi-processing technology. Specifically, before the online tracking, two parallel processes P_1, P_2 are initiated. This initialization also includes a shared flag $Flag$ and variable V to synchronize status and transmit data between processes. At each frame t , P_1 filters raw detections while P_2 concurrently predicts the previous alive trajectory and implements online tracking. After completing their respective tasks, P_1 and the prediction part of P_2 enter a sleep state, remaining dormant until they are simultaneously awakened in the subsequent frame. Fast-Poly

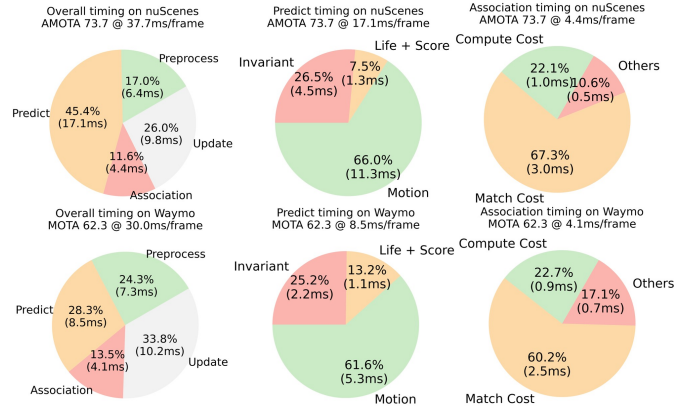


Fig. 4: The average timing statistics of each module in Fast-Poly on the nuScenes and Waymo val set without parallelization. **Invariant** means the lightweight filter for time-invariant states. **Motion** means the Kalman Filter for motion states. **Life** means the lifecycle module. **Score** means the score refinement. adheres to online tracking principles and fundamentally differs from [4], which employs multi-processing for synchronous multi-scene tracking.

IV. EXPERIMENTS

A. Dataset and Implementation Details

nuScenes. nuScenes [8] provides intricate scenes and numerous short sequences (40 frames) with 2Hz for keyframe data. Evaluation encompasses 7 categories: Car (*Car*), Bicycle (*Bic*), Motorcycle (*Moto*), Pedestrian (*Ped*), Bus (*Bus*), Trailer (*Tra*), and Truck (*Tru*). The primary evaluation metric is AMOTA [10]. Fast-Poly is conducted utilizing only keyframes.

Waymo. Waymo [9] provides extended sequences (approximately 20 seconds each) for tracking Vehicle (*Veh*), Cyclist (*Cyc*), and Pedestrian (*Ped*), captured at a frequency of 10Hz. The main evaluation metric, MOTA [21], is categorized into two levels based on the LiDAR points in labels: LEVEL_1 and LEVEL_2. MOTA on LEVEL_2 is reported due to the cumulative nature of difficulty levels.

Implementation Details. Under Python implementation with NumPy [33], Fast-Poly is deployed and tested. We perform the linear search to refine the optimal AMOTA (nuScenes) and MOTA (Waymo) hyperparameters on the validation set. The best hyperparameters are subsequently utilized on the test set. SF thresholds are category-specific and detector-specific, which are (*Moto, Car, Bic*: 0.16; *Bus, Tra*: 0.13; *Tru*: 0; *Ped*: 0.19) on nuScenes, (*Veh*: 0.8; *Ped, Cyc*: 0.84) on Waymo. The NMS thresholds are 0.08 on all categories and datasets. With default IoU_{bev} in NMS, we additionally utilize our proposed $A-gIoU_{bev}$ to describe similarity for (*Bic, Ped, Bus, Tru*) on nuScenes, (*Veh, Ped, Cyc*) on Waymo. The motion models and filters are consistent with [1]. The lightweight filter is implemented by the median filter with $l_{lw} = 3$ on all datasets. The association metrics are all implemented by $A-gIoU$ on all datasets. The first association thresholds θ_{fm} are category-specific, which are (*Bic, Moto*: 1.6; *Bus, Car, Tra, Tru*: 1.2; *Ped*: 1.8) on nuScenes, (*Veh*: 1.1; *Ped*: 1.3; *Cyc*: 1.2) on Waymo. Voxel mask size θ_{vm} is 3m on nuScenes and 5m on Waymo. The count-based and

TABLE I: A comparison between our proposed method with other advanced methods on the nuScenes test set. This leaderboard is available at [nuScenes official benchmark](#). ‡ means the GPU device. The reported runtimes of all methods exclude the detection time. Fast-Poly and [1] rely entirely on the detector input, as they do not utilize any visual or deep features during tracking.

Method	Device	Detector	Input	AMOTA↑	MOTA↑	FPS↑	IDS↓	FN↓	FP↓
EagerMOT [3]	–	CenterPoint [19]&Cascade R-CNN [34]	2D+3D	67.7	56.8	4	1156	24925	17705
CBMOT [14]	17-9700	CenterPoint [19]&CenterTrack [20]	2D+3D	67.6	53.9	80.5	709	22828	21604
Minkowski [5]	TITAN‡	Minkowski [5]	3D	69.8	57.8	3.5	325	21200	19340
ByteTrackv2 [16]	–	TransFusion-L [35]	3D	70.1	58	–	488	21836	18682
3DMOTFormer [15]	2080Ti‡	BEVFusion [24]	2D+3D	72.5	60.9	54.7	593	20996	17530
Poly-MOT [1]	9940X	LargeKernel3D [25]	2D+3D	75.4	62.1	3	292	17956	19673
Fast-Poly (Ours)	7945HX	LargeKernel3D [25]	2D+3D	75.8	62.8	34.2	326	18415	17098

TABLE II: A comparison of the average time consumption of each step of GIoU and our proposed metric A-GIoU in data association on nuScenes val set. **Overlap** means solving intersections. **Convex** means solving convex hulls.

Metric	Overall	Overlap	Convex	Others
$gIoU$	111.3ms	24.7ms	83.0ms	3.6ms
$A-gIoU$	0.0098ms	0.0033ms	0.0016ms	0.0049ms

TABLE III: A comparison of the run-time performance on different devices on nuScenes val set with CenterPoint.

Device	Level	FPS↑	AMOTA↑	MOTA↑
Ryzen9 7945HX	Personal	28.9	73.7	63.2
Intel 9940X	Server	13.4		
Cortex A78AE	Embedded	8.7		

output file strategies are consistent with [1]. In the confidence-based part, decay rates σ are category-specific, which are (*Moto*, *Ped*: 0.6; *Car*, *Tra*: 0.5; *Tru*: 0.2; *Bus*: 0.3; *Bic*: 0.1) on nuScenes, (*Veh*: 0.6; *Ped*: 0.7; *Cyc*: 0.1) on Waymo. The delete threshold θ_{dl} are (*Bus*, *Ped*: 0.1 and 0.04 for other categories) on nuScenes, (*Cyc*: 0.2; *Veh*, *Ped*: 0.1) on Waymo.

Metrics. We present three primary indicators: MOTA [21], AMOTA [10], and FPS (Frame Per Second), supplemented by three secondary indicators: IDS (ID Switch), FP, and FN. The latency of each experiment is the average time cost under multiple evaluations. We only measure the tracking time for all methods, excluding the detection time.

B. Run-time Discussion

The comparison with other methods. As shown in Tables I and IV, our inference speed is extremely competitive on both datasets. We outline the detailed time consumption of each module in Figure 4 and Table II. On nuScenes, Fast-Poly can run at 34.2 FPS without any GPU. Besides, the association timing is significantly reduced to 4.4ms, which accounts for only 4% of the original $gIoU$ calculation time. Due to the higher-quality detections (due to the differing requirements between MOTA and AMOTA), the overall timing (35.5 FPS) as well as that of each module is further reduced for the Waymo dataset. The estimation module dominates the latency, constituting 60% of the total, largely due to the computational demands of solving the Jacobian matrix in the EKF.

The robustness of device migration. As demonstrated in Table III, we evaluated Fast-Poly across three CPU tiers. Since our method is learning-free, tracking accuracy remains unaffected by device migration. On the personal-level CPU, Fast-Poly exhibits the best real-time performance (29 FPS). Furthermore, without engineering acceleration, Fast-Poly can

TABLE IV: A comparison between our proposed method with other advanced methods on the Waymo val and test set. The leaderboard is available at [Waymo official benchmark](#). The inference speed is 35.5 FPS.

Split	Method	Detector	Input	MOTA↑
Val	CenterPoint [19]	CenterPoint [19]	3D	55.8
	SimpleTrack [4]	CenterPoint [19]		56.9
	CasTrack [36]	CasA [26]		61.3
	Fast-Poly (Ours)	CasA [26]		62.3
Test	PVRCNN-KF [27]	PVRCNN [27]	3D	55.5
	CenterPoint [19]	CenterPoint [19]		58.7
	SimpleTrack [4]	CenterPoint [19]		60.2
	CasTrack [36]	CasA [26]		62.6
	Fast-Poly (Ours)	CasA [26]		63.6

achieve nearly real-time performance (9 FPS) on limited CPU resources (Jetson Orin AGX), highlighting its practicality.

The parallel efficiency of Fast-Poly. As depicted in Fig. 1, when the number of objects increases significantly, the frame timing of Fast-Poly exhibits minimal increments (≤ 30 ms), highlighting the outstanding computational efficiency and feasibility of our method in autonomous driving scenarios.

C. Comparative Evaluation

nuScenes. Fast-Poly establishes a new state-of-the-art performance on the test set, with 75.8% AMOTA and 34.2 FPS, surpassing all existing methods. With the same detector, Fast-Poly outperforms Poly-MOT [1] on all major metrics (accuracy: +0.4% AMOTA and +0.7% MOTA, latency: +31.2 FPS). Despite being marginally slower than CBMOT [14] and 3DMOTFormer [15] in speed, Fast-Poly significantly outperforms them in accuracy. On a limited computing platform (only personal CPU), Fast-Poly maintains high accuracy and high real-time consistency. Our method is open-sourced, serving as a strong baseline for 3D MOT.

On the val set, we employ CenterPoint [19] as the detector for a fair comparison. As shown in Table VII, Fast-Poly outperforms most learning-based/free methods by a significant margin in terms of both tracking accuracy (73.7% AMOTA, 64.2% MOTA) and latency (29 FPS). We surpass the baseline [1] with a notable improvement of +1.3% in MOTA and +0.6% in AMOTA accuracy, while 5 \times faster under identical settings. Fast-Poly exhibits stronger tracking performance with a powerful detector LargeKernel3D [25]. Utilizing the multi-camera detector DETR3D [37] with constrained performance, Fast-Poly shows robust real-time performance and accuracy, exceeding the end-to-end tracker PF-Track (+4.5% AMOTA) and TBD tracker CC-3DT [38] (+4.8% AMOTA). Notably, Poly-MOT requires a strict score filter threshold to achieve optimal AMOTA, reducing the latency advantage of our method.

TABLE V: The ablation studies of each module on the nuScenes val. **AG** means A-GIoU. **VM** means Voxel Mask. **LW** means LightWeight Filter. **CL** means Confidence-Count Mixed Lifecycle. **MP** means Multi-Processing.

Index	Alignment				Parallelization	Primarily Metric			Secondary Metric		
	AG	VM	LW	CL	MP	AMOTA \uparrow	MOTA \uparrow	FPS \uparrow	IDS \downarrow	FP \downarrow	FN \downarrow
Baseline [1]	-	-	-	-	-	73.1	61.9	5.6 (188.7ms)	232	13051	17593
Exp1	✓	-	-	-	-	73.1	62.4	19.9 (50.3ms)	342	13955	16794
Exp2	✓	✓	-	-	-	73.3	63.0	21.3 (46.9ms)	385	12732	17909
Exp3	✓	✓	✓	-	-	73.3	62.9	21.7 (46.1ms)	427	14124	16523
Exp4	✓	✓	✓	✓	-	73.7	63.2	26.5 (37.7ms)	414	14713	15900
Exp5	✓	✓	✓	✓	✓	73.7	63.2	28.9 (34.6ms)	414	14713	15900

TABLE VI: A comparison on distinct lifecycle modules on nuScenes val set. **Average** means using the online average score to delete. **Latest** means using the latest score to delete. **Max-age** means using the continuous mismatch time to delete. Other settings are under the best performance.

Strategy	AMOTA \uparrow	MOTA \uparrow	FPS \uparrow	FN \downarrow
Count & Max-age	73.3	62.9	23.0	16523
Confidence [14] & Latest	70.6	63.2	45.8	19192
Confidence [14] & Average	73.3	63.1	28.3	16826
Confidence (Ours) & Average	73.7	63.2	28.9	15900

TABLE VII: A comparison between our proposed method with other advanced methods on the nuScenes val set. ‡ means the GPU device. All metrics in the competition papers are reported. Methods in lines 1-7, lines 8-9, and line 10-13 use CenterPoint [19], LargeKernel3D [25] and DETR3D [37].

Method	Device	AMOTA \uparrow	MOTA \uparrow	FPS \uparrow	IDS \downarrow
OGR3MOT [7]	TITANXp‡	69.3	60.2	12.3	262
SimpleTrack [4]	9940X	69.6	60.2	0.5	405
3DMOTFormer [15]	2080Ti‡	71.2	60.7	54.7	341
ByteTrackv2 [16]	-	72.4	62.4	-	183
ShaSTA [6]	A100‡	72.8	-	10.0	-
Poly-MOT [1]	7945HX	73.1	61.9	5.6	232
Fast-Poly (Ours)	7945HX	73.7	63.2	28.9	414
Poly-MOT [1]	7945HX	75.2	54.1	8.6	252
Fast-Poly (Ours)	7945HX	76.0	65.8	34.2	307
CC-3DT [38]	3090‡	35.9	32.6	9.6	2152
PF-Track [18]	A100‡	36.2	-	-	300
Poly-MOT [1]	7945HX	38.7	32.3	16.3	926
Fast-Poly (Ours)	7945HX	40.7	33.1	39.3	1312

Waymo. As shown in Table IV, with the same detector, we exceed CasTrack [12] with a +1% improvement in MOTA on both sets, showcasing superior tracking performance. Without using the state-of-the-art detector, Fast-Poly ranks 4th on the Waymo tracking leaderboard among all LiDAR-only online methods with 63.6% MOTA to date. Despite the scarcity of methods showcasing real-time performance on Waymo, we believe that our inference speed (35.5 FPS) is competitive.

D. Ablation Studies

To verify the effectiveness of each module, we conducted comprehensive ablation experiments on the nuScenes val set. Our baseline tracker Poly-MOT [1] is re-implemented with the official code. With baseline detector CenterPoint [19], the best performance for each ablation experiment is reported.

The effect of the Proposed Metric A-GIoU. As demonstrated in Tables II and V, *A-gIoU* results in a significant reduction in latency (-138.4ms), particularly during the overlap (-24.7ms) and convex hull (-83ms) calculations. *A-gIoU* maintains AMOTA (73.1%) while improving MOTA (+0.5%). Fig. 3(a) shows this refinement stems from focusing on tight positional correlations, recalling more observations (-799 FN).

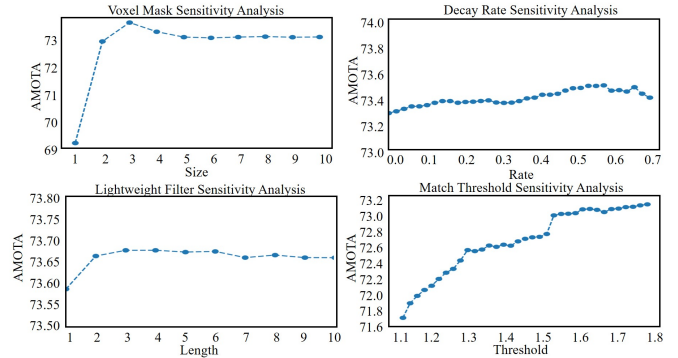


Fig. 5: The comparison of the accuracy under distinct newly introduced hyperparameter. No category-specific technique is performed, all categories are applied the same parameter.

The effect of the Voxel Mask. As illustrated in Table V, the voxel mask improves overall accuracy (+0.2% AMOTA, +0.6% MOTA) and reduces latency (-3.4ms), verifying its effectiveness in avoiding invalid cost calculations. Specifically, it enhances absolute position constraints, preventing wrong matches from redundant detections (-1223 FP).

The effect of the Lightweight Filter. Table V indicates combining the lightweight filter enhances real-time performance (-0.8ms). However, the inner limited-step sliding window discards long-term temporal information for time-invariant states, slightly impacting estimation quality and overall tracking accuracy (-0.1% MOTA).

The effect of the Confidence-Count Mixed Lifecycle. Table V shows our lifecycle module (EXP4) increases processing speed by 4.8 FPS over EXP3, indicating more efficient tracklet management. It also improved AMOTA and MOTA by 0.4% and 0.3% respectively, validating its efficacy. As shown in Table VI, our tracklet termination strategy (line 3) outperforms the original score refinement [14] (line 2) with a 2.7% AMOTA increase and 2366 fewer FN, boosting tracker robustness against mismatch scenarios (occlusion, etc.). The smoother score prediction (line 4) further enhances tracking performance (+0.4% AMOTA, +0.1% MOTA, -926 FN).

The effect of the Parallelization. Without compromising accuracy or violating online tracking principles, the multi-processing parallelization effectively alleviates the inherent serial logic of the TBD framework and improves the inference speed by 8.2% (-3.1ms).

E. Hyperparameter Sensitivity Analysis

The plethora of hand-crafted hyperparameters poses a fundamental limitation to the TBD framework. In response, we

conduct a sensitivity analysis on newly introduced hyperparameters on the nuScenes val set. Retaining other parameters, the linear search rule is executed for filter length l_{lw} , voxel mask size θ_{vm} , decay rate σ and match threshold θ_{fm} . A critical finding in Fig. 5 is that Fast-Poly showcases insensitivity to all parameters except θ_{fm} , with an average fluctuation of less than 0.4% in AMOTA. The pronounced decrease in θ_{vm} at 1 stems from erroneous matches induced by artificially narrowing the matching space. Furthermore, θ_{fm} emerges as a pivotal factor for all trackers, manifesting sensitivity across categories [1], [3], [16]. These findings underscore the resilience of our proposed method in parameter selection. The optimal hyperparameters are delineated in Section IV-A.

V. CONCLUSION

In this work, we proposed an efficient and powerful polyhedral framework for 3D MOT, termed Fast-Poly. To ensure consistency in both accuracy and latency, Fast-Poly integrates three core principles to enhance the baseline Poly-MOT, including: (1) Alignment: By aligning objects, our proposed A-GIoU addresses the detrimental effect of 3D rotation on similarity calculation. (2) Densification: Through soft lifecycle management, voxel mask, and lightweight filter, we enhance the computational efficiency of trajectory maintenance, cost matrix construction, and filter estimation, respectively. (3) Parallelization: Based on multi-processing technology, we perform parallel the prediction and pre-processing modules, effectively alleviating the serial defects of the TBD framework. We conduct extensive experiments on two large-scale tracking benchmarks. Fast-Poly achieves state-of-the-art performance (75.8% AMOTA and 34.2 FPS) among all methods on nuScenes and demonstrates superior real-time and accuracy performance (63.6% MOTA and 35.5 FPS) on Waymo. Fast-Poly is open source and hopes to contribute to the community.

REFERENCES

- [1] X. Li, T. Xie, D. Liu, J. Gao, K. Dai, Z. Jiang, L. Zhao, and K. Wang, "Poly-mot: A polyhedral framework for 3d multi-object tracking," in *IROS*. IEEE, 2023, pp. 9391–9398.
- [2] L. Wang, X. Zhang, W. Qin, X. Li, J. Gao, L. Yang, Z. Li, J. Li, L. Zhu, H. Wang *et al.*, "Camo-mot: Combined appearance-motion optimization for 3d multi-object tracking with camera-lidar fusion," *T-ITS*, 2023.
- [3] A. Kim, A. Osep, and L. Leal-Taixé, "Eagermot: 3d multi-object tracking via sensor fusion," in *ICRA*. IEEE, 2021, pp. 11 315–11 321.
- [4] Z. Pang, Z. Li, and N. Wang, "Simpletrack: Understanding and rethinking 3d multi-object tracking," in *ECCVW*. Springer, 2022, pp. 680–696.
- [5] J. Gwak, S. Savarese, and J. Bohg, "Minkowski tracker: A sparse spatio-temporal r-cnn for joint object detection and tracking," *arXiv preprint arXiv:2208.10056*, 2022.
- [6] T. Sadjapour, J. Li, R. Ambrus, and J. Bohg, "Shasta: Modeling shape and spatio-temporal affinities for 3d multi-object tracking," *RA-L*, 2023.
- [7] J.-N. Zaech, A. Liniger, D. Dai, M. Danelljan, and L. Van Gool, "Learnable online graph representations for 3d multi-object tracking," *RA-L*, vol. 7, no. 2, pp. 5103–5110, 2022.
- [8] H. Caesar, V. Bankiti, A. H. Lang, S. Vora, V. E. Liong, Q. Xu, A. Krishnan, Y. Pan, G. Baldan, and O. Beijbom, "nuscenes: A multimodal dataset for autonomous driving," in *CVPR*, 2020, pp. 11 621–11 631.
- [9] P. Sun, H. Kretzschmar, X. Dotiwalla, A. Chouard, V. Patnaik, P. Tsui, J. Guo, Y. Zhou, Y. Chai, B. Caine *et al.*, "Scalability in perception for autonomous driving: Waymo open dataset," in *CVPR*, 2020, pp. 2446–2454.
- [10] X. Weng, J. Wang, D. Held, and K. Kitani, "3d multi-object tracking: A baseline and new evaluation metrics," in *IROS*. IEEE, 2020, pp. 10 359–10 366.
- [11] X. Wang, C. Fu, Z. Li, Y. Lai, and J. He, "Deepfusionmot: A 3d multi-object tracking framework based on camera-lidar fusion with deep association," *RA-L*, vol. 7, no. 3, pp. 8260–8267, 2022.
- [12] H. Wu, W. Han, C. Wen, X. Li, and C. Wang, "3d multi-object tracking in point clouds based on prediction confidence-guided data association," *T-ITS*, vol. 23, no. 6, pp. 5668–5677, 2021.
- [13] C. Liu, H. Li, and Z. Wang, "Fasttrack: A highly efficient and generic gpu-based multi-object tracking method with parallel kalman filter," *IJCV*, pp. 1–21, 2023.
- [14] N. Benbarka, J. Schröder, and A. Zell, "Score refinement for confidence-based 3d multi-object tracking," in *IROS*. IEEE, 2021, pp. 8083–8090.
- [15] S. Ding, E. Rehder, L. Schneider, M. Cordts, and J. Gall, "3dmotformer: Graph transformer for online 3d multi-object tracking," in *ICCV*, 2023, pp. 9784–9794.
- [16] Y. Zhang, X. Wang, X. Ye, W. Zhang, J. Lu, X. Tan, E. Ding, P. Sun, and J. Wang, "Bytrackv2: 2d and 3d multi-object tracking by associating every detection box," 2023.
- [17] T. Zhang, X. Chen, Y. Wang, Y. Wang, and H. Zhao, "Mutr3d: A multi-camera tracking framework via 3d-to-2d queries," in *CVPR*, 2022, pp. 4537–4546.
- [18] Z. Pang, J. Li, P. Tokmakov, D. Chen, S. Zagoruyko, and Y.-X. Wang, "Standing between past and future: Spatio-temporal modeling for multi-camera 3d multi-object tracking," in *CVPR*, 2023, pp. 17 928–17 938.
- [19] T. Yin, X. Zhou, and P. Krahenbuhl, "Center-based 3d object detection and tracking," in *CVPR*, 2021, pp. 11 784–11 793.
- [20] X. Zhou, V. Koltun, and P. Krähenbühl, "Tracking objects as points," in *ECCV*. Springer, 2020, pp. 474–490.
- [21] K. Bernardin, A. Elbs, and R. Stiefelhagen, "Multiple object tracking performance metrics and evaluation in a smart room environment," in *Sixth IEEE International Workshop on Visual Surveillance, in conjunction with ECCV*, vol. 90, no. 91. Citeseer, 2006.
- [22] J. Luiten, A. Osep, P. Dendorfer, P. Torr, A. Geiger, L. Leal-Taixé, and B. Leibe, "Hota: A higher order metric for evaluating multi-object tracking," *IJCV*, vol. 129, pp. 548–578, 2021.
- [23] J. Huang, G. Huang, Z. Zhu, Y. Ye, and D. Du, "Bevdet: High-performance multi-camera 3d object detection in bird-eye-view," *arXiv preprint arXiv:2112.11790*, 2021.
- [24] Z. Liu, H. Tang, A. Amini, X. Yang, H. Mao, D. L. Rus, and S. Han, "Bevfusion: Multi-task multi-sensor fusion with unified bird's-eye view representation," in *ICRA*. IEEE, 2023, pp. 2774–2781.
- [25] Y. Chen, J. Liu, X. Qi, X. Zhang, J. Sun, and J. Jia, "Scaling up kernels in 3d cnns," *arXiv preprint arXiv:2206.10555*, 2022.
- [26] H. Wu, J. Deng, C. Wen, X. Li, C. Wang, and J. Li, "Casa: A cascade attention network for 3-d object detection from lidar point clouds," *T-GRS*, vol. 60, pp. 1–11, 2022.
- [27] S. Shi, C. Guo, L. Jiang, Z. Wang, J. Shi, X. Wang, and H. Li, "Pv-rnn: Point-voxel feature set abstraction for 3d object detection," in *CVPR*, 2020, pp. 10 529–10 538.
- [28] H. W. Kuhn, "The hungarian method for the assignment problem," *Naval research logistics quarterly*, vol. 2, no. 1-2, pp. 83–97, 1955.
- [29] I. E. Sutherland and G. W. Hodgman, "Reentrant polygon clipping," *Communications of the ACM*, vol. 17, no. 1, pp. 32–42, 1974.
- [30] R. L. Graham, "An efficient algorithm for determining the convex hull of a finite planar set," *Info. Proc. Lett.*, vol. 1, pp. 132–133, 1972.
- [31] H. Rezatofighi, N. Tsoi, J. Gwak, A. Sadeghian, I. Reid, and S. Savarese, "Generalized intersection over union: A metric and a loss for bounding box regression," in *CVPR*, 2019, pp. 658–666.
- [32] C. Bai, T. Xiao, Y. Chen, H. Wang, F. Zhang, and X. Gao, "Faster-lid: Lightweight tightly coupled lidar-inertial odometry using parallel sparse incremental voxels," *RA-L*, vol. 7, no. 2, pp. 4861–4868, 2022.
- [33] S. Van Der Walt, S. C. Colbert, and G. Varoquaux, "The numpy array: a structure for efficient numerical computation," *Computing in science & engineering*, vol. 13, no. 2, pp. 22–30, 2011.
- [34] Z. Cai and N. Vasconcelos, "Cascade r-cnn: Delving into high quality object detection," in *CVPR*, 2018, pp. 6154–6162.
- [35] X. Bai, Z. Hu, X. Zhu, Q. Huang, Y. Chen, H. Fu, and C.-L. Tai, "Transfusion: Robust lidar-camera fusion for 3d object detection with transformers," in *CVPR*, 2022, pp. 1090–1099.
- [36] H. Wu, W. Han, C. Wen, X. Li, and C. Wang, "3d multi-object tracking in point clouds based on prediction confidence-guided data association," *T-ITS*, vol. 23, no. 6, pp. 5668–5677, 2021.
- [37] Y. Wang, V. C. Guizilini, T. Zhang, Y. Wang, H. Zhao, and J. Solomon, "Detr3d: 3d object detection from multi-view images via 3d-to-2d queries," in *CoRL*. PMLR, 2022, pp. 180–191.
- [38] T. Fischer, Y.-H. Yang, S. Kumar, M. Sun, and F. Yu, "Cc-3dt: Panoramic 3d object tracking via cross-camera fusion," 2022.